

01,07,09,19

First-Principles Study of the Physical Properties of CuV_2S_4 under Pressure

© M. Atikur Rahman¹, J.F. Lubna¹, S. Sarker¹, R. Khatun¹, S. Kumur Saha¹, M.Z. Rahaman², K.M. Hossain³, M. Rasheduzzaman⁴, M.Z. Hasan⁴

¹ Department of Physics, Pabna University of Science and Technology, Pabna-6600, Bangladesh

² School of Materials Science and Engineering, Faculty of Science, University of New South Wales, Sydney 2052, Australia

³ Department of Materials Science and Engineering, University of Rajshahi, Rajshahi-6205, Bangladesh

⁴ Department of Electrical and Electronic Engineering, International Islamic University Chittagong, Kumira, Chittagong-4318, Bangladesh

E-mail: atik0707phy@gmail.com

Received Januari, 15, 2022

Revised April, 7, 2022

Accepted April, 8, 2022

The structural, electronic, mechanical, thermodynamic, and optical properties of CuV_2S_4 have been studied under pressure (0–50 GPa) by employing first-principles computation depending on the density functional theory. The optimized structural constraints are in good accord with the experimental results. By employing different pressure, the variation of single crystal elastic constant C_{ij} as well as polycrystalline mechanical parameters are evaluated and discussed in detail. The increment of elastic constant with the increase in pressure guaranteed that CuV_2S_4 turn ought to be more resilient to shear distortion with pressure. The linear response of elastic moduli under pressure confirms that hardness of CuV_2S_4 rises with increasing pressure. The Pugh's ratio ensured the ductile nature of CuV_2S_4 . Band structure and DOS calculations have been confirmed the electrically conductive nature of CuV_2S_4 . The population analysis validates the presence of dominant covalent bonding. Optical properties, *i.e.*, absorption, conductivity, reflectivity, and loss function are also explored with the variation of pressure. These optical functions demonstrate that the compound exhibits high reflectivity in the low-energy range, which assures the application of this compound as coating material. The thermodynamic properties are also investigated under pressure and discussed.

Keywords: first-principles study, spinel-type compound CuV_2S_4 , mechanical properties, electronic properties, optical and thermal properties.

DOI: 10.21883/PSS.2022.08.54607.003

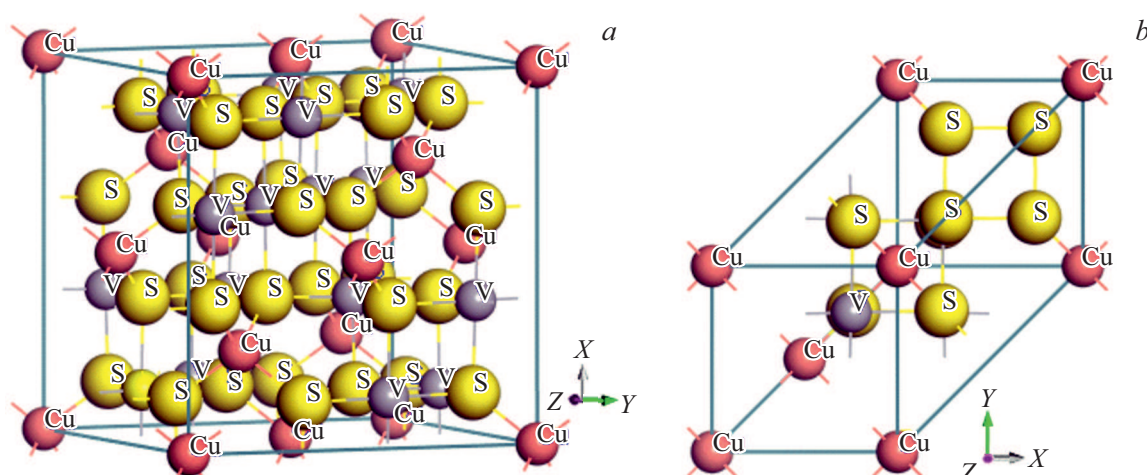
1. Introduction

Various research teams are interested in chalcogenide spinel compounds because of their excellent physical characteristics, such as magnetic ordering and the metal-insulator transition [1–4]. In the technical implementation, spinel compounds are used. For high-energy laser systems, the spinel-based transparent ceramics were sketched recently [5]. Highly efficient luminescent materials have been documented on the basis of the spinel compounds [6–8]. Spinel is also used in diagnostics as fluorescence markers [9]. We focus on one representative of the thiospinel subgroup (here thio belongs to sulfur) with the chemical formula CuV_2S_4 . This is a chalcogenide spinel belonging to the family of AB_2X_4 (A and B denote the transition metals), and X denotes a chalcogen. A ion hold the tetrahedral sites and B ion hold the octahedral sites in these types of chalcogenide spinels which have a normal cubic structure. Further, formation of a network of corner sharing tetrahedral by B -sub-lattice is defined as a geometrically frustrated

pyrochlore lattice. Geometrical dissatisfaction is a common characteristic due to spin-ice state, spin-liquid state, charge and orbital ordering, the development of spin clusters, and heavy fermion-like manners [10–13]. At room temperature, CuV_2S_4 is one of such identical substances exhibiting phase transition at 90 and 50 K [14,15]. The exceptional properties of the metallic thiospinel CuV_2S_4 has been revealed between 50 and 90 K in the X-ray diffraction (XRD) pattern [14], resistivity [14], magnetic susceptibility [16], and specific heat [17]. In CuV_2S_4 , the superconductivity may be caused by the compression of charge density waves. The highest superconductivity was initiated in LiTi_2O_4 which is a spinel iso-structural compound. S. Ramakrishnan *et al.* explored the lock-in transitions and charge density wave of CuV_2S_4 [18]. J.V. Waszczak *et al.* discussed the magnetic properties of copper chalcogenide spinels. They stated CuV_2S_4 as unique spinel chalcogenide with excellent magnetic properties. Lu *et al.* conducted the XPS and XES measurements of CuV_2S_4 and validated their results with the density functional theory (DFT) investigations [19].The

Table 1. Calculated equilibrium lattice parameter a_0 , unit cell volume V_0 , bulk modulus B_0 of CuV_2S_4 at zero pressure

Properties	Expt.	Other calculation [experiment]	Present calculation	Deviation from other result
a_0 , Å	9.779 [19]	9.8203 [16]	9.755	0.45%
V_0 , Å ³	–	–	928.286	–
B_0 , GPa	–	–	112.07	–

**Figure 1.** Crystal structures of CuV_2S_4 : a) conventional unit cell, b) optimized cell.

CuV_2S_4 compound crystallizes in the face-centered-cubic Al_2MgO_4 -type structure with space group of Fd-3m at room temperature. Due to phase transitions below 100 K, the symmetry of CuV_2S_4 is lower [20].

Pressure's effect on the physical properties of the CuV_2S_4 spinel compound has not been performed yet, as far as we know. Even the optical and elastic properties under zero pressure have not been explored. Hence, the structural, elastic, electronic, thermodynamic, and optical characteristics of CuV_2S_4 in the pressure range from 0 to 50 GPa as well as electronic properties under zero pressure are studied and discussed thoroughly by DFT means.

2. Computational methods

The current investigations have been accomplished by applying the CASTEP code dependent on the density functional theory [21–24]. Taking advantage of the GGA within the method presented by PBE, the electronic exchange–correlation interactions have been treated [24]. The Vanderbilt-type ultra-soft pseudo-potentials for Cu, V, and S atoms have been used [25]. The pseudo-atomic calculations are executed for $\text{Cu-}3d^{10}4s^1$, $\text{V-}3s^23p^63d^34s^2$, and $\text{S-}3s^23p^4$. The plane wave cutoff energy is used for all physical properties calculations and that has set to 400 eV. For generating $12 \times 12 \times 12$ k-point grids for the sampling of the Brillouin zone, Monkhorst–Pack method has been employed [26]. The geometrical optimizations have been achieved by using BFGS minimization

method [27]. The total energy convergence parameters are set as $2.0 \cdot 10^{-5}$ eV/atom, 0.05 V/Å for the maximum Hellmann–Feynman force, 0.002 Å for the maximum ionic displacement, 0.01 GPa for the maximum stress, and the maximum iteration is within 100. Under the conditions of each pressure (0 to 50 GPa) at the optimized structure, the elastic stiffness constants of the cubic crystal CuV_2S_4 have been found using the stress–strain approach [28]. In case of the investigation of polycrystalline elastic constants, Voigt and Reuss approximation have been adopted.

3. Results and discussion

3.1. Structural properties

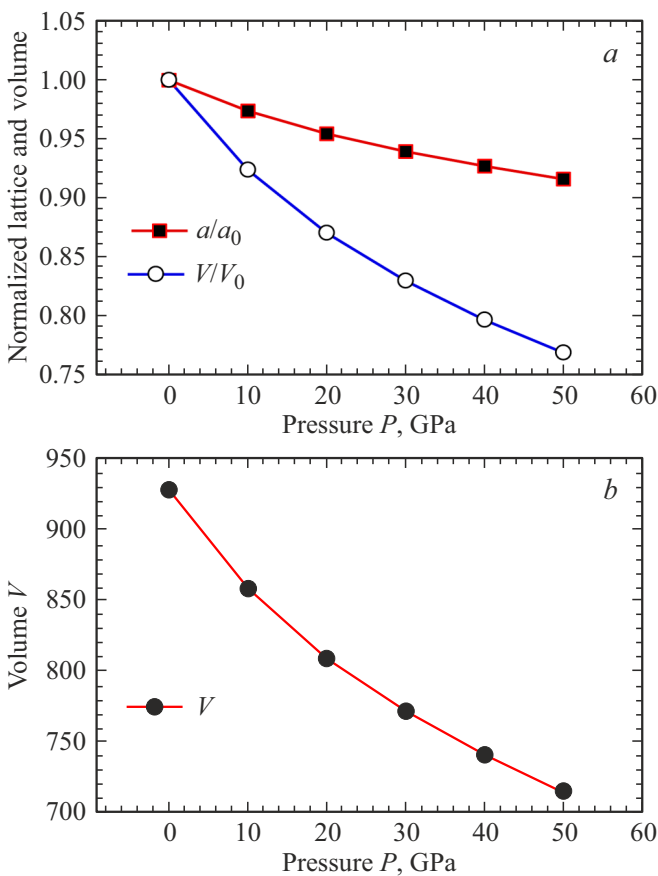
The thiospinel CuV_2S_4 possesses Al_2MgO_4 type cubic crystal structure of space group Fd-3m (227). The space group of Fd-3m reflects the symmetry of CuV_2S_4 above 100 K [20]. Fourteen atoms are contained by the unit cell with two formula units. The optimized equilibrium crystal structure is attained by limiting the total energy with reference to lattice constant and internal atomic positions. The Wyckoff positions occupying by the spinel-type compound, CuV_2S_4 are 8a (0, 0, 0) for Cu, 16d (0.625, 0.625, 0.625) for V, and 32e (0.3807, 0.3807, 0.3807) [19]. In Fig. 1, the conventional and optimized structures of the spinel have shown. Table 1 demonstrates the estimated structural parameters along with the available experimental and previous theoretical values.

Table 2. Calculated lattice parameter a and unit cell volume V of CuV_2S_4 compound under pressure

Pressure P , GPa	Lattice parameter a , Å	Cell volume V , Å ³
0	9.755	928.29
10	9.502	857.86
20	9.316	808.61
30	9.169	771.07
40	9.047	740.46
50	8.941	714.83

The estimated lattice parameters are found to be very proximate to both experimental and previous theoretical values. The investigated lattice parameter reveals 0.45% divergence in contrast with the experimental value and somewhat different from previous theoretical values owing to the temperature reliance of cell parameters and GGA process [29], which ensure the reliability of our DFT-based calculations. We do not do temperature-based DFT calculations.

For examining the impact of external pressure on the crystal structure of CuV_2S_4 , the changes of the lattice parameters and unit cell volume have been studied. The

**Figure 2.** a) Normalized lattice parameters and b) the unit cell volume vs pressure for compound CuV_2S_4 .

investigated structural parameters at different hydrostatic pressures are recorded in Table 2.

The normalized lattice parameter and volume of CuV_2S_4 as a function of pressure are illustrated in Fig. 2, *a* and *b*. It is observed that with the increase of pressure, the normalized lattice parameter a/a_0 and normalized volume V/V_0 are decreased (where a_0 and V_0 stand for the equilibrium lattice parameter and volume under zero pressure). This happens because as pressure is increased; the repulsive interaction of Cu, V, and S atoms is strengthened, resulting in the bond length of these atoms reduction. As a result, as pressure increases, the lattice parameter decreases. As presented in Fig. 2, *b*, the unit cell volume decreases with increasing pressure for the decrement of lattice parameters.

3.2. Elastic properties

The elastic constants that interact with the mechanical and dynamical characteristics of a solid are the fundamental factors of any solid material. These constants are used to describe mechanical stability of solid and to link the relationship between phonon spectrum and Debye temperature of crystals. Any compound's elastic properties are roughly connected to its long-wavelength phonon spectrum, hence superconducting material's elastic properties must be explored [30]. A comprehensive analysis of elastic characteristics for materials is also crucial for understanding the chemical bonding character between adjacent atoms and the material's cohesion [31].

As a result, understanding the mechanical characteristics of CuV_2S_4 and its behavior under pressure a comprehensive investigation of the elastic constants is needed. Hook's law [32] is used to determine the elastic constants by applying the stress-strain function. CuV_2S_4 exhibits three separate elastic constants (C_{11} , C_{12} , and C_{44}) like a cubic crystal [33]. For the first time the investigated elastic constants for CuV_2S_4 under pressure are listed in Table 3.

All three constants must reach the following Born stability requirements [34] in order for a cubic structure to be stable. These criteria are

$$C_{11} > 0, C_{44} > 0, C_{11} - C_{12} > 0, \text{ and } C_{11} + 2C_{12} > 0. \quad (1)$$

The examined elastic constants are positive from 0 to 50 GPa and fulfill the aforesaid stability requirements, implying that the CuV_2S_4 is mechanically stable up to 50 GPa, as seen in Table 3. There are currently no more theoretical data for the elastic constants of CuV_2S_4 . As a result, we are unable to contrast our findings to other theoretical data.

Fig. 3 represents the pressure effect of elastic constants of CuV_2S_4 . From this figure, we have noticed that the elastic constants C_{11} and C_{12} increases linearly with increasing pressure. Whereas the variation of C_{44} indicates that the cubic structure is in unstable phase and the phase transition may take place at high pressure.

Table 3. Calculated elastic constants C_{ij} of CuV_2S_4 compound under pressure

Compounds	Pressure P, GPa	C_{11} , GPa	C_{12} , GPa	C_{44} , GPa	Ref.
CuV_2S_4	0	167.68	84.27	43.27	This study
CuRh_2S_4		129.25	94.67	30.23	[35]
CuRh_2Se_4		120.78	81.51	19.47	
CuV_2S_4	10	207.84	127.46	44.06	This study
	20	243.91	171.10	43.10	
	30	266.66	208.25	40.17	
	40	300.36	247.31	40.81	
	50	325.01	283.50	40.18	

Mechanical parameters such as bulk modulus B , Young’s modulus E , shear modulus G , anisotropy factor A , and Poisson’s ratio ν are crucial for understanding material’s mechanical behavior. As a result, it is necessary to understand how these factors change under pressure. We have applied Voigt–Reuss–Hill (VRH) equating approach to computing these parameters [36]. Using the formulae given below, for any cubic crystal, the Voigt and Reuss bounds of B and G have been derived [37].

$$B_V = B_R = \frac{C_{11} + 2C_{12}}{3}, \tag{2}$$

$$G_V = \frac{(C_{11} - C_{12} + 3C_{44})}{5}, \tag{3}$$

$$G_R = \frac{5C_{44}(C_{11} - C_{12})}{[4C_{44} + 3(C_{11} - C_{12})]}. \tag{4}$$

As per Hill, the average value of B and G can be stated as

$$B = \frac{1}{2}(B_R + B_V), \tag{5}$$

$$G = \frac{1}{2}(G_V + G_R). \tag{6}$$

Hill’s bulk and shear moduli (B_H and $G + H$) can be utilized to compute Young’s modulus E and Poisson’s ratio ν [38].

$$E = \frac{9GB}{3B + G}, \tag{7}$$

$$\nu = \frac{3B - 2G}{2(3B + G)}. \tag{8}$$

It is also important to calculate the Zener anisotropy in solid [39] and found by the equation below,

$$A = \frac{2C_{44}}{(C_{11} - C_{12})}. \tag{9}$$

The evaluated data of bulk modulus B , shear modulus G , B/G values, Young’s modulus E , Poisson’s ratio ν , and anisotropy factor A are shown in Table 4.

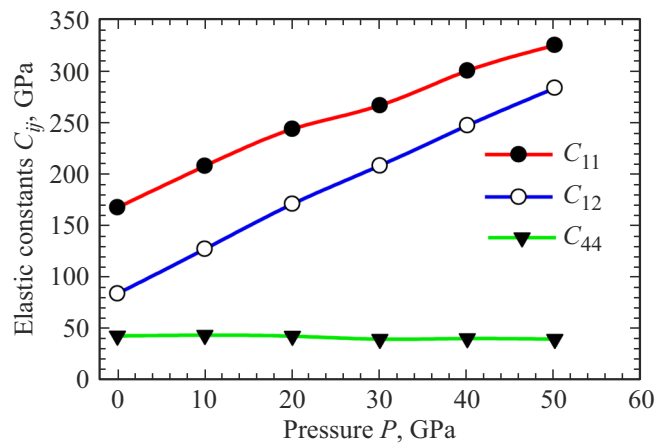
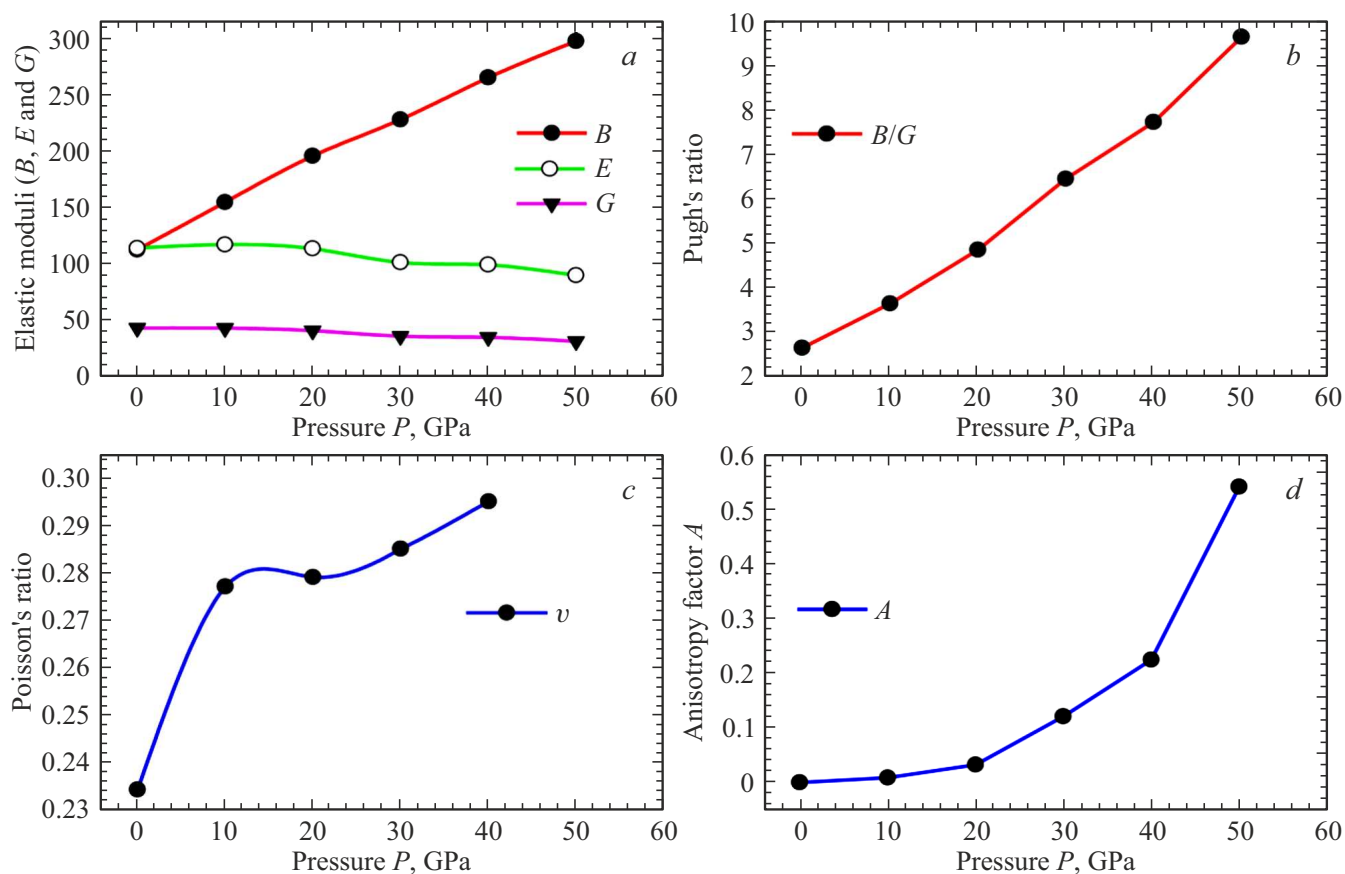


Figure 3. Pressure dependence of elastic constants C_{ij} (C_{11} , C_{12} , and C_{44}) for CuV_2S_4 .

Bulk modulus B is used to assess resistance to volume changes, while shear modulus G is used to assess resistance to shape changes. Young’s modulus E , on the other hand, is used to determine material stiffness. The large value of Young’s modulus ensures the hardness of the material. According to Fig. 4, a , we have observed that the value of bulk modulus increases with increasing pressure, which suggests that the capability to prevent the deformation of CuV_2S_4 is increased with increasing pressure. Elsewhere, the decrease of G and E with increasing pressure reflects the capability to prevent the shear deformation. From Fig. 4, a , we have observed that the value of G and E are decreased with increasing pressure. The decrease of these parameters denotes the happening structural or electronic phase transition with pressure. For each material, the critical value of Pugh’s ratio is 1.75, which distinguishes between crystals that are ductile (> 1.75) and brittle (< 1.75) [40]. Since the values of Pugh’s ratio of CuV_2S_4 at different pressures are greater than 1.75 and increase with pressure as shown in Table 4, we can say that the ductile nature of CuV_2S_4 increases with increasing pressure. The graphical

Table 4. Calculated bulk modulus B , shear modulus G , B/G values, Young's modulus E , Poisson's ratio ν , and anisotropy factor A for CuV_2S_4 compound under pressure

Compounds	Pressure P , GPa	B	G	E	B/G	ν	A	Ref.
CuV_2S_4	0	112.07	42.64	113.52	2.63	0.340	0.0016	This study
CuRh_2S_4		106.20	25.05	69.67	4.23	0.39	1.74	[35]
CuRh_2Se_4		94.60	19.53	54.81	4.84	0.40	0.99	[35]
CuV_2S_4	10	154.26	42.47	116.70	3.63	0.374	0.0102	This study
	20	195.37	40.29	113.09	4.84	0.404	0.0343	
	30	227.72	35.35	100.83	6.44	0.426	0.1228	
	40	264.99	34.34	98.75	7.72	0.438	0.2263	
	50	297.34	30.83	89.40	9.64	0.450	0.5429	


Figure 4. a) Variation of the bulk modulus B , shear modulus G , Young's modulus E ; b) Pugh ratio B/G ; c) variation of Poisson's ratio ν ; and d) anisotropy factor A of CuV_2S_4 under pressure.

representations of variations of Pugh's ratio are shown in Fig. 4, b. As per the Frantsevich rule [41], if the Poisson's ratio is less than 0.33, a material should act as brittle or ductile.

Our investigation revealed that CuV_2S_4 has a ductile character since the computed value of Poisson's ratio ν is more than 0.33, and the value of Poisson's ratio increases

with rising pressure (Fig. 4, c). So, we can say that the ductile nature also increases with pressure. The anisotropy factor's unit value ($A = 1$) represented a fully isotropic material, while a value more or less than unity ($A < 1$ or $A > 1$) denoted the extent of elastic anisotropy. The substance CuV_2S_4 demonstrated an anisotropic response under pressure, as seen in Table 4.

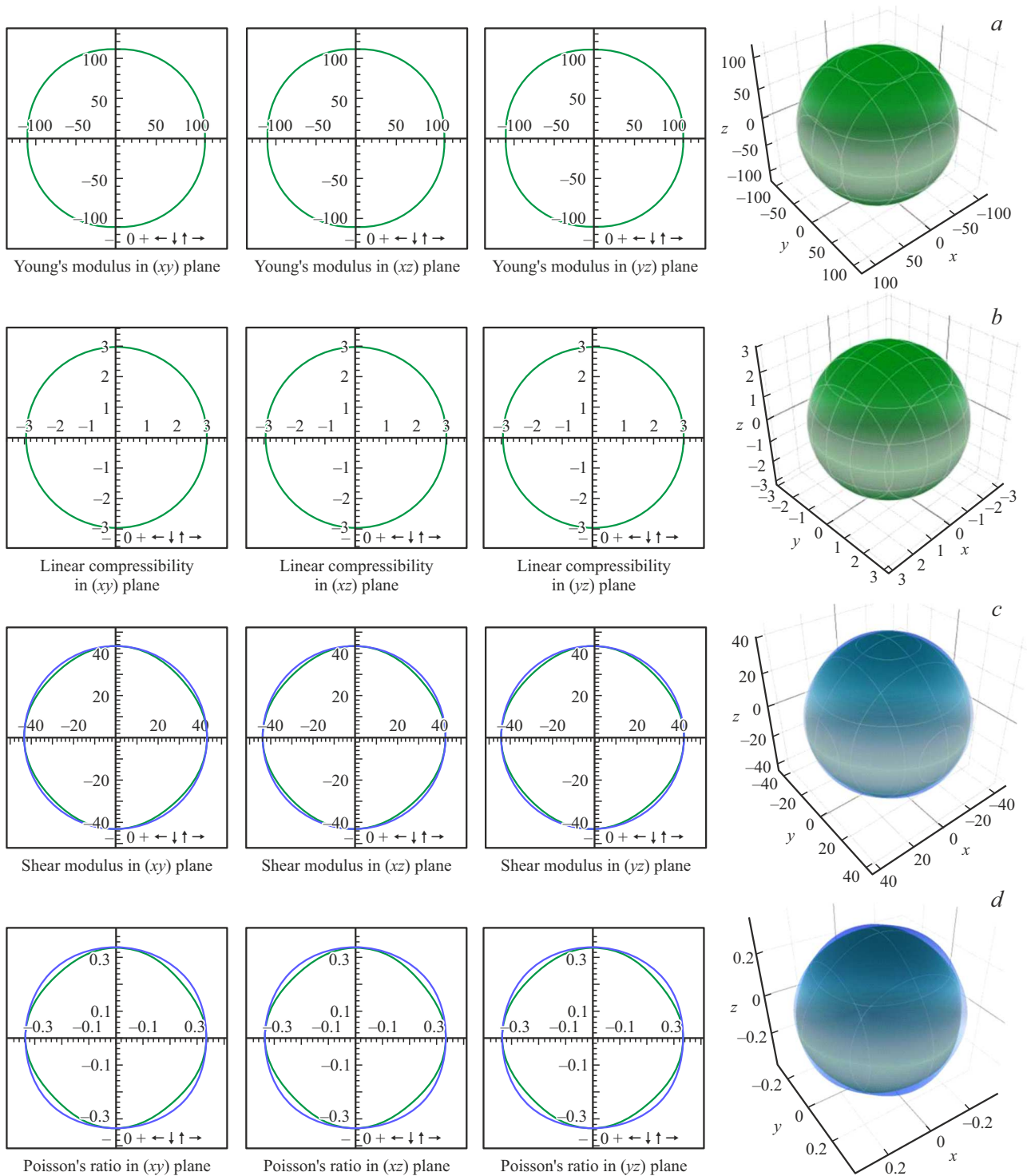


Figure 5. 2D and 3D plots of a) Young’s modulus E , b) compressibility K , c) shear modulus G , and d) Poisson’s ratio ν of CuV_2S_4 at 0 GPa.

3.3. Anisotropic characteristics

By plotting the values in 2D and 3D presentations, the direction dependencies of Young’s modulus, compressibility, shear modulus, and Poisson’s ratio are studied using the ELATE code [43]. From the behavior of the profiles of the

3D and 2D planar projection plots of the elastic moduli and elastic constants, the anisotropy can be understood. Completely circular (2D) as well as spherical (3D) profiles are waited for isotropic solids otherwise, it can be treated as the degree of anisotropy. At 0 GPa, the direction dependence of Young’s modulus E , compressibility K , shear

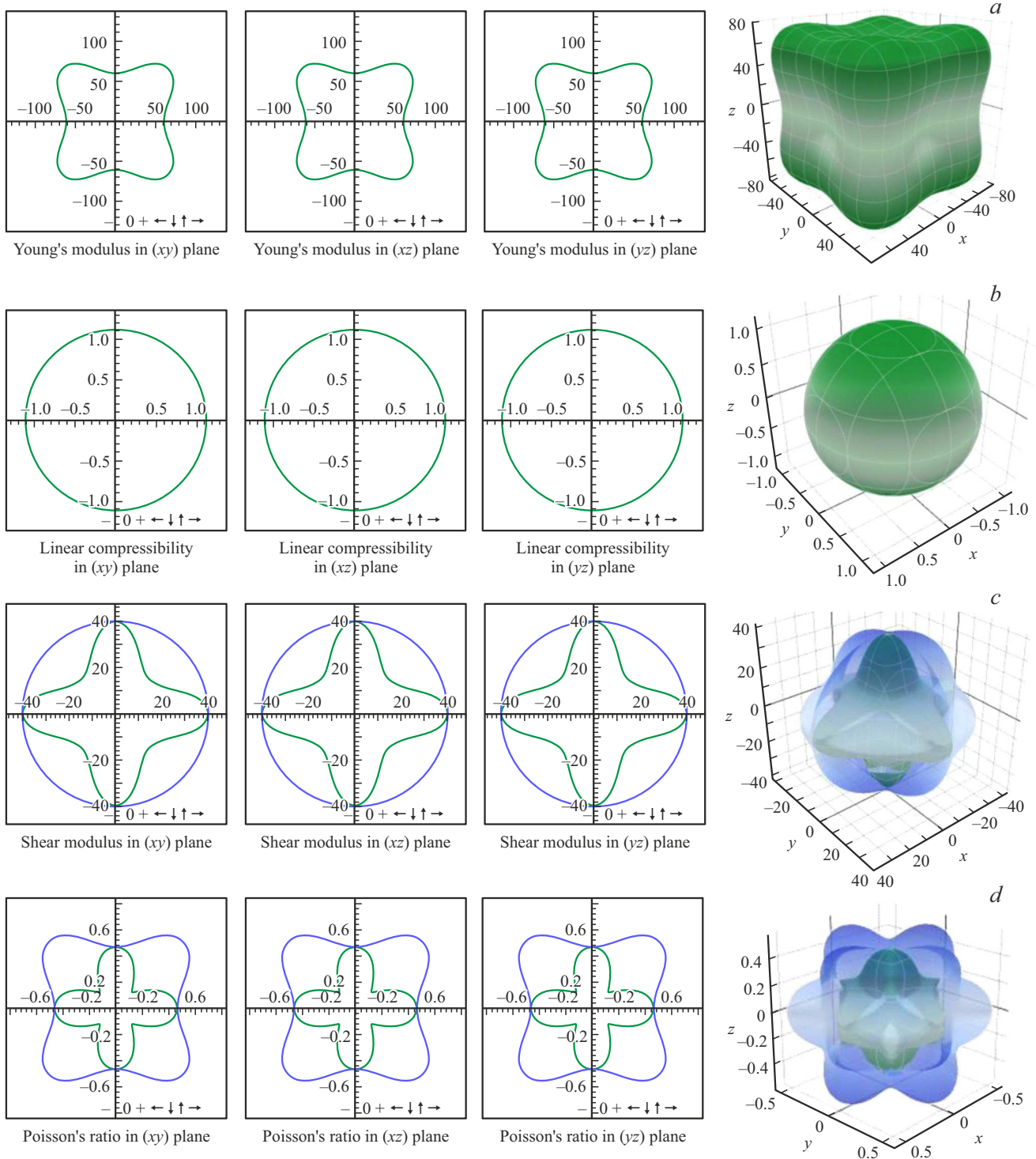


Figure 6. 2D and 3D plots of a) Young's modulus E , b) compressibility K , c) shear modulus G , and d) Poisson's ratio ν of CuV_2S_4 at 50 GPa.

modulus G , and Poisson's ratio ν are depicted in Fig. 5, $a-d$. Fig. 6, $a-d$ represent the 2D and 3D configuration of Young's modulus E , compressibility K , shear modulus G , and Poisson's ratio ν of CuV_2S_4 at 50 GPa.

The minimum and maximum values of E , K , G , and ν of CuV_2S_4 are enlisted in Table 5.

The anisotropy carries momentous interest owing to its close relation with a number of important physical processes [42].

We observed from Fig. 5, a that the deviation from circular shape presentation of E in the xy , xz and yz plane assures its anisotropic nature. E is minimum (111.32 GPa)

Table 5. The minimum and the maximum values of the Young's modulus, compressibility, shear modulus, and Poisson's ratio of CuV_2S_4

P , GPa	E_{\min} , GPa	E_{\max} , GPa	A_E	K_{\min} , TPa	K_{\max} , TPa	A_K	G_{\min} , GPa	G_{\max} , GPa	A_G	ν_{\min}	ν_{\max}	A
0	111.32	115.01	1.03	2.974	2.974	1	41.71	43.27	1.04	0.318	0.343	1.078
10	110.94	120.71	1.09	2.161	2.161	1	40.19	44.07	1.09	0.340	0.405	1.190
20	102.82	120.45	1.17	1.706	1.706	1	36.40	43.10	1.18	0.339	0.463	1.363
30	84.03	113.81	1.35	1.464	1.464	1	29.21	40.16	1.38	0.301	0.546	1.810
40	77.01	116.46	1.51	1.258	1.258	1	26.52	40.81	1.54	0.265	0.605	2.287
50	60.85	115.35	1.89	1.121	1.121	1	20.76	40.18	1.94	0.173	0.722	4.176

Table 6. Mulliken atomic populations of CuV_2S_4 under pressure

Pressure P , GPa	Species	s	p	d	Total	Charge	Bond	Population	Lengths, Å
0	S	1.80	4.35	0.00	6.15	-0.15	S-Cu	0.56	2.20424
	V	2.42	6.54	3.80	12.76	0.24	S-V	0.46	2.38676
	Cu	0.55	0.61	9.71	10.87	0.13			
50	S	1.74	4.26	0.00	6.00	0.00	S-Cu	0.76	1.98325
	V	2.36	6.48	4.12	12.96	0.04	S-V	0.49	2.20831
	Cu	0.51	0.91	9.66	11.09	-0.09			

and E is maximum at 45° (115.01 GPa) of all planes; the anisotropic ratio is, therefore, 1.03. Similarly, from Fig. 5, b we observed that a circular presentation of compressibility K assures its isotropic nature in all planes. As seen from Fig. 5, c , the shear modulus G in the all plane assures its slightly anisotropic nature because its shape is not perfectly circular. G is minimum (111.32 GPa) and G is maximum at 45° (115.01 GPa) of all planes; the anisotropic ratio is, therefore, 1.04. Like the shear modulus, Poisson's ratio also shows the anisotropy nature in the all plane. We see from Fig. 6 that with the rising of pressure, the circular shapes are deviated and it is also evident that the compound CuV_2S_4 showed completely anisotropic behavior under pressure.

3.4. Electronic properties

The analysis of electronic characteristics is crucial because it helps us comprehend the electronic structure of materials [44]. The computed electronic band structure is represented in Fig. 7. The dotted line has been considered as Fermi level.

It is noticeable that the valence band and conduction band overlap each other at Fermi level. It is an indication of the metallic nature of CuV_2S_4 . Fig. 8 depicts the total and partial density of states that were explored.

The DOS of CuV_2S_4 compound at 0 GPa in the range from -20 to 5 eV are represented in Fig. 8. TDOS is represented at various pressure in Fig. 9. The role of TDOS and DOS at the Fermi level also indicate the metallic nature of CuV_2S_4 . The Cu $3d$, V $3p$ and S $3s$ states come up with the significant role to construct the valence band where

V $3d$ states come up with the significant role to construct the conduction band (Fig. 8). At Fermi level, the TDOS for CuV_2S_4 is 10 states per unit cell per eV. The largest peak in the valence band is at -36 to -40 eV, which is entirely made up of V $3d$ states and is not depicted in the image. The TDOS of CuV_2S_4 at various pressure is shown in Fig. 9. It's worth noting that when pressure rises, the contribution of DOS at Fermi level decreases.

Mulliken populations of CuV_2S_4 have been investigated to understand the bonding properties [45]. Mulliken population is an essential criterion for analyzing ionic or covalent behavior of bonds. The evaluated bond parameters of CuV_2S_4 are displayed in Table 6. A zero value of population reveals perfect ionic bond, negative value reveals an anti-bonding state, while the positive value reveals rising covalency [46].

From Table 6, we have investigated that V atom carries positive charge for both 0 and 50 GPa pressure. In case of S atom, we have noticed that it carries negative charge at 0 GPa but holds positive charge at 50 GPa pressure. The other atom Cu carries positive charge at 0 GPa but carries negative charge at 50 GPa pressure. Further, we can see that the bond population of S-Cu and S-V bonds is positive for both 0 and 50 GPa pressure, which refers to the presence of covalent bond in CuV_2S_4 .

3.5. Optical properties

A frequency dependent dielectric function, which is given by the following equation, is used to express the optical

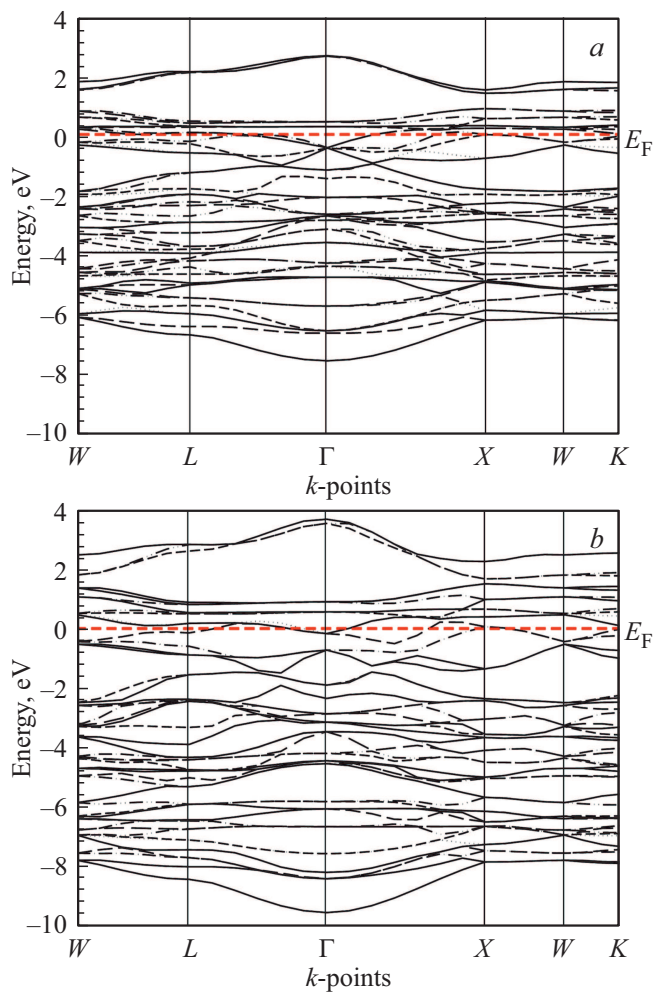


Figure 7. Electronic band structure of CuV_2S_4 at *a*) 0 GPa and *b*) 50 GPa.

characteristics.

$$\varepsilon(\omega) = \varepsilon_1(\omega) + i\varepsilon_2(\omega), \quad (10)$$

where ω is the frequency of light, $\varepsilon_1(\omega)$ reflects the real part of the dielectric function, and $\varepsilon_2(\omega)$ reflects the imaginary part. The imaginary component can be stated using momentum matrix elements and by examining all potential transitions between the occupied and unoccupied electronic states which is given by the equation below [47–49].

$$\varepsilon_2(\omega) = \frac{2e^2\pi}{V\varepsilon_0} \sum_{k,v,c} |\langle \psi_{ck} | \mathbf{u} \cdot \mathbf{r} | \psi_{vk} \rangle|^2 \delta(E_k^c - E_k^v - E), \quad (11)$$

where the integral is over the first Brillouin zone. Here, ω denotes the frequency of the photon, e refers to the electronic charge, V stands for the unit cell volume, \mathbf{u} is the unit vector along the polarization of the incident electric field, and ψ_{ck} and ψ_{vk} represent the wave functions for conduction and valence band electrons at a particular k , respectively. Since CuV_2S_4 has metallic nature, as validated by the predicted band structure calculations, a

Drude term [50] with plasma frequency 4 eV and Drude damping 0.05 eV has been used. The calculated optical functions of CuV_2S_4 are recorded in Fig. 10 from 0 to 50 eV energy range. For all the computations, we have used 0.5 eV

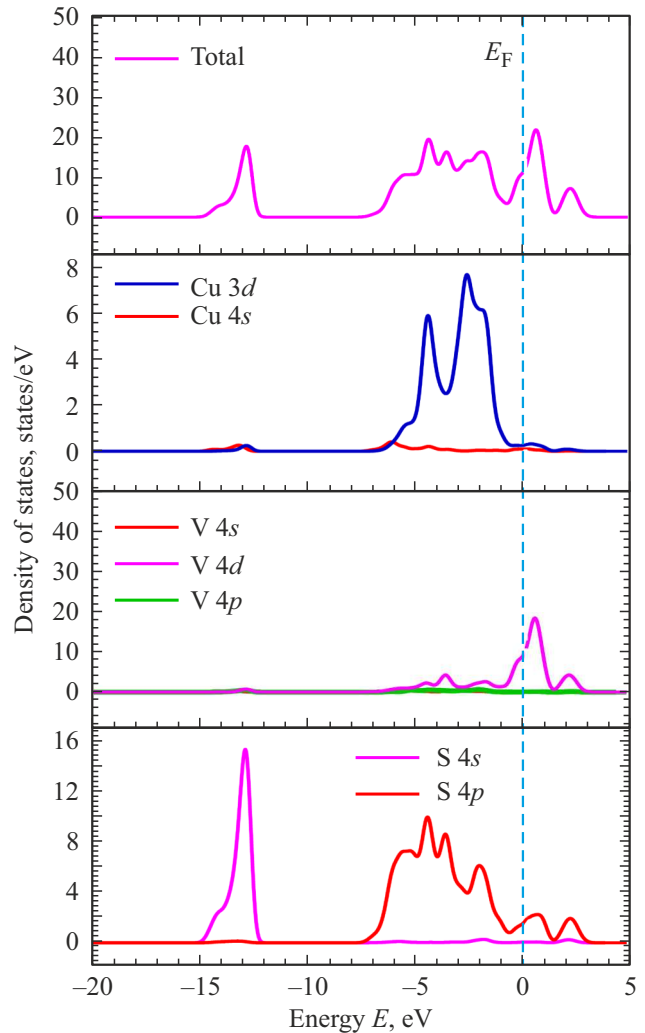


Figure 8. The total density of states and partial density of states of CuV_2S_4 compound under zero pressure.

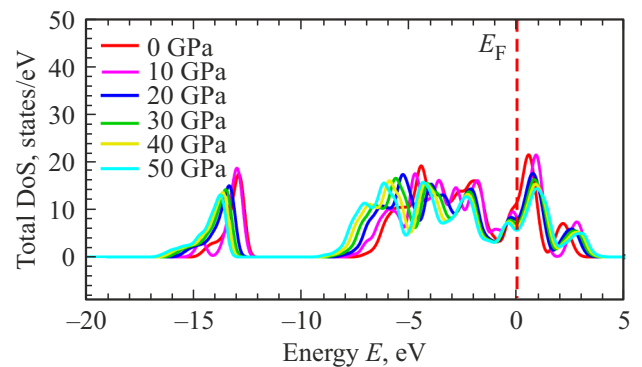


Figure 9. The total density of states of CuV_2S_4 compound at various pressures.

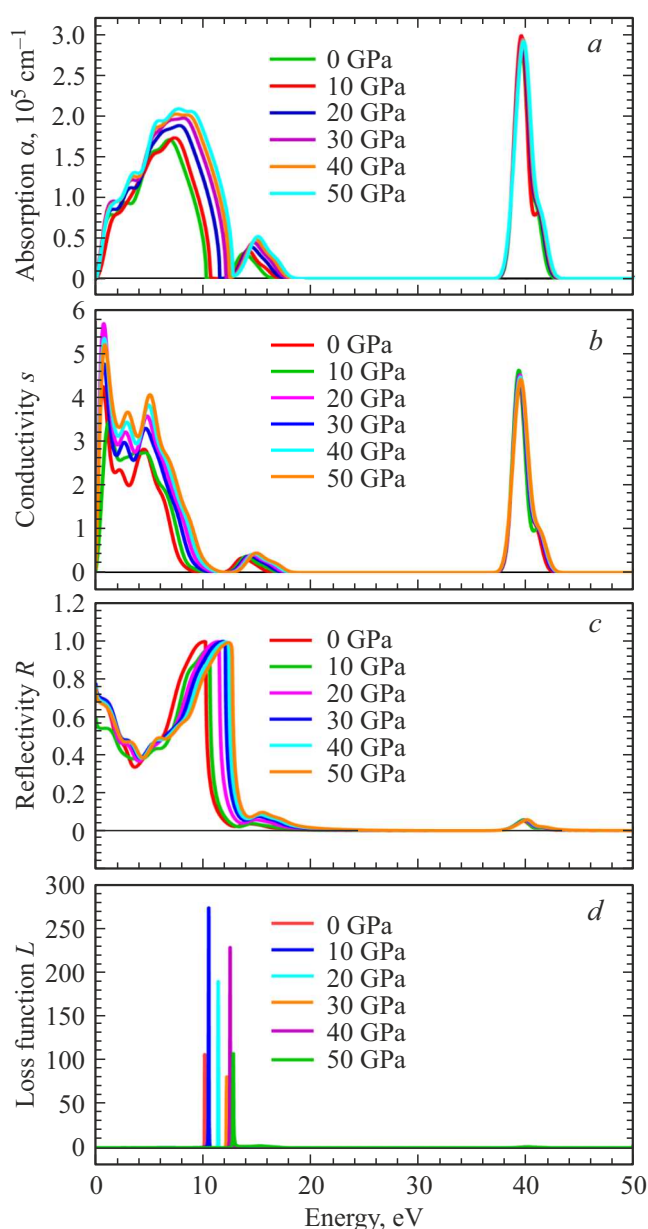


Figure 10. The pressure-dependent *a*) absorption, *b*) conductivity, *c*) reflectivity, and *d*) loss function of CuV_2S_4 .

Gaussian smearing, since this spreads out the Fermi plane; thus the k -points will be more efficient at the Fermi surface.

The absorption coefficient is a significant factor which delivers the understanding of best solar energy conversion efficiency. It represents the light with a certain energy that can go through the material before being entirely absorbed [51]. It is clear that the absorption coefficient starts out with zero photon energy because of its metallic nature. The highest peaks are investigated which are situated at the energy range 38 to 42 eV. This compound demonstrated excellent absorption coefficient. From Fig. 10, *a* we can see that if we increase pressure, the absorption coefficient is increased which is ensured from the changes of the positions

and height of peaks. From this study, we also can observe that CuV_2S_4 compound retain decent absorption coefficient in the ultraviolet zone.

When an alternating electric field is present, optical conductivity becomes electrical conductivity. The real components of optical conductivity under various pressures are demonstrated in Fig. 10, *b*. It is observed that under all the pressure, the optical conductivity commences from zero photon energy that further implies the metallic character of the studied compound. From the band structure it has also been ensured. A wide range of incident photon energy can be used to generate the photocurrent. We investigated that the maximum peaks of the compound depended on pressure. Unique case is for 30 GPa. In this study, at first the electrical conductivity increased in between the energy range from 0 to 1 eV then it decreased with further pressure increase. Again, we got the increased peaks under pressure in the energy range 38 to 42 eV.

Fig. 10, *c* represents the reflectivity spectra R of CuV_2S_4 as a function of photon energy. From the figure, we have investigated that reflectivity started with a value of 0.58–0.77 for 0 to 50 GPa, then decreased and again increased having a maximum value in between the energy range 9.99 to 12.43 eV. After that, the reflectivity again decreased. If the value of reflectivity is large at very small energies then it indicates the higher dynamic conductivity in that region.

The energy loss of a fast electron moving through a substance is represented by the loss function. The frequency connected to the upper limit of the energy loss spectrum is specified by the bulk plasma frequency ω_p of the material, which emerges at $\epsilon_2 < 1$ and $\epsilon_1 = 0$ [52]. Fig. 10, *d* shows the loss function at various pressure. In the energy range where the loss function is highest, there we investigated the marginal optical conductivity, reflectivity, and absorption. The highest peaks located at 10.23, 10.67, 11.48, 12.28, 12.59, and 12.89 eV for 0 to 50 GPa, as shown in Fig. 10, *d*. The variable peaks are found for specific pressure because of shear anisotropy. The material appears translucent if the plasma frequency is lower than its respective incident light.

3.6. Thermodynamic properties

The temperature which is connected to the highest frequency mode of vibration is called Debye temperature. This is the fundamental lattice dynamical parameter having a distinctive temperature of solid materials. Debye temperature relates to various physical properties, *e.g.*, thermal conductivity, thermal expansion, lattice vibration, melting temperature, specific heat, etc. Two essential factors, *i.e.*, critical temperature and electron–phonon coupling constant can be correlated by Debye temperature. Debye temperature of a material can be evaluated by using various data, including the elastic moduli. In this present study, we use elastic modulus data for the calculation of Debye temperature. By using the following equations, the Debye

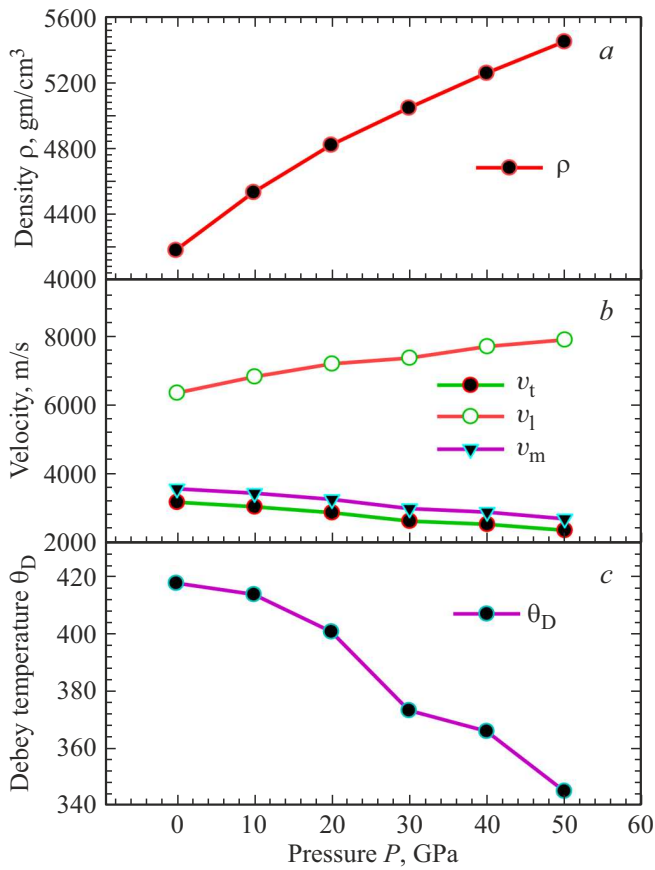


Figure 11. Pressure-dependent a) density, b) velocities, and c) Debye temperature of CuV_2S_4 compound.

temperature has been estimated [53–57],

$$\theta_D = \frac{h}{k_B} \left[\left(\frac{3n}{4\pi} \right) \left(\frac{N_A \rho}{M} \right) \right]^{1/3} \cdot v_{av}, \quad (12)$$

$$v_{av} = \left[1/3 \left(\frac{2}{v_t^3} + \frac{1}{v_l^3} \right) \right]^{-1/3}, \quad (13)$$

$$v_l = \left(\frac{3B + 4G}{3\rho} \right)^{1/2}, \quad (14)$$

$$v_t = \left(\frac{G}{\rho} \right)^{1/2}, \quad (15)$$

where h and k_B are the Planck's and Boltzman constant, N_A is the Avogadro's number, ρ is the density, M is represented as the molecular weight and n is the number of atoms contained in the unit cell of CuV_2S_4 . Furthermore, v_{av} is the average elastic (sound) wave velocity which is used in the equation of Debye temperature calculation. v_{av} can be determined by using the value of v_t and v_l which are mentioned in the equation below. v_t and v_l are known as the transverse and longitudinal sound velocities.

The evaluated values of v_l , v_t , v_{av} , ρ , and Debye temperature θ_D have been displayed in Table 7. The average velocity is decreasing with the increment of pressure for

Table 7. The evaluated density ρ , transverse sound velocity v_t , longitudinal sound velocity v_l , average sound velocity v_{av} , and Debye temperature θ_D of CuV_2S_4 under pressure

Pressure, GPa	ρ , kg/m ³	v_t , m/s	v_l , m/s	v_{av} , m/s	θ_D , K
0	4190	3190.08	6349.47	3577.65	417.63
10	4540	3058.53	6815.48	3449.94	413.67
20	4826	2891.17	7188.77	3274.44	400.72
30	5050	2645.75	7359.32	3005.53	373.42
40	5260	2555.10	7686.54	2907.17	366.13

Table 8. The calculated melting temperature T_m and the minimum thermal conductivity κ_{min} of CuV_2S_4 compound under various pressure

Pressure P , GPa	κ_{min} , $\text{Wm}^{-1}\text{K}^{-1}$	T_m , K
0	0.758	1543.99
10	0.771	1781.33
20	0.762	1994.51
30	0.721	2128.96
40	0.716	2328.13
50	0.684	2473.81

CuV_2S_4 compound. From Fig. 11, c it is apparent that the Debye temperature is decreasing with the rising of pressure. We can also observe that CuV_2S_4 is thermally less conductive under pressure.

Melting temperature is defined as the temperature at which a material alters its state to liquid at ambient pressure and this fact is well-known as melting point of solid. Fine

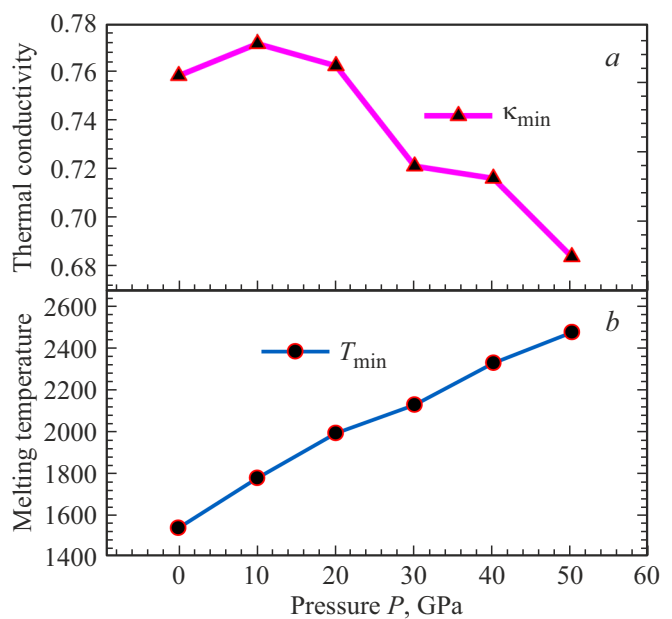


Figure 12. Pressure-dependent a) minimum thermal conductivity and b) melting temperature.

et al. suggested the following empirical equation for cubic substance, which is applied to compute the melting temperature [58]:

$$T_m = 553 + 5.91C_{11}. \quad (16)$$

Table 8 and Fig. 12 illustrated the melting temperature at various pressure.

The melting temperature of this substance increased as pressure was raised, as seen in Fig. 12, *b*. Hence; this material can be used as a good structural material.

The minimum thermal conductivity κ_{\min} is a property of solid material that describes the behavior of atoms within a crystal when the material is heated or cooled. κ_{\min} can be estimated by using average sound velocity which is represented in the following equation [59]:

$$\kappa_{\min} = k_B v_{\text{av}} \left(\frac{nN_{\text{A}}\rho}{M} \right)^{2/3}. \quad (17)$$

The symbols employed in this equation have the same interpretation as the symbols presented in equation (12). The value of minimum thermal conductivity as a function of pressure is listed in Table 8 and shown in Fig. 12, *a*.

4. Conclusions

Using density functional theory (DFT), the precise physical characteristics of the CuV_2S_4 compound at different pressures are explored. The optimized structural parameters accorded well with the available experimental data at zero pressure. The normalized structural parameters a/a_0 and V/V_0 are diminished with the influence of pressure. The investigated three independent elastic constants guaranteed that CuV_2S_4 is mechanically stable. The polycrystalline elastic parameters are increased with increasing pressure. Moreover, CuV_2S_4 is characterized as ductile material and the hardness and ductility are increased with pressure since the Pugh's ratio is increasing with pressure. In contrast, with increasing pressure, the decrement of G and E denoted that the ability to resist the shear deformation of CuV_2S_4 is decreased. This material also exhibits the increase of anisotropy factor with pressure. CuV_2S_4 's metallic character is confirmed by DOS and band structure analyses. The total density of states is decreased when the pressure is increased. The existence of covalent bonds is observed in CuV_2S_4 based on the Mulliken atomic populations. The study of optical properties also ensured the metallic nature of CuV_2S_4 . The Debye temperature is decreased with the increase in pressure. Finally, the enhanced melting temperature is observed with increasing pressure.

Conflicts of interests

The authors declare that they have no conflict of interest.

References

- [1] F.K. Lotgering. On the ferrimagnetism of some sulphides and oxides. PhD thesis, Utrecht University (1956).
- [2] S. Nagata, T. Hagino, Y. Seki, and T. Bitoh. *Physica B* **194–196**, 1077 (1994).
- [3] P.G. Radaelli, Y. Horibe, M.J. Gutmann, H. Ishibashi, C.H. Chen, R.M. Ibberson, Y. Koyama, Y.-S. Hor, V. Kiryukhin, and S.-W. Cheong. *Nature* **416**, 6877, 155 (2002).
- [4] T. Hagino, Y. Seki, N. Wada, S. Tsuji, T. Shirane, K. Kumagai, and S. Nagata. *Phys. Rev. B* **51**, 18, 12673 (1995).
- [5] J. Sanghera, Shyam Bayya, G. Villalobos, W. Kim, J. Frantz, B. Shaw, B. Sadowski, R. Miklos, C. Baker, M. Hunt, I. Aggarwal, F. Kung, D. Reicher, S. Peplinski, A. Ogloza, P. Langston, C. Lamar, P. Varmette, M. Dubinskiy, and L. DeSandre. *Opt. Mater.* **33**, 3, 511 (2011).
- [6] L. Suchow and N.R. Stemple. *J. Electrochem. Soc.* **111**, 2, 191 (1964).
- [7] P.J. Dereń, K. Maleszka-Bagińska, P. Gluchowski, and M.A. Małecka. *J. Alloys. Comp.* **525**, 39 (2012).
- [8] A. Watras, P.J. Dereń, R. Pązik, K. Maleska-Bagińska. *Opt. Mater.* **34**, 12, 2041 (2012).
- [9] C. Alvarez-Lorenzo, L. Bromberg, and A. Concheiro. *Photochem. Photobiology* **85**, 4, 848 (2009).
- [10] S.-H. Lee, C. Broholm, W. Ratcliff, G. Gasparovic, Q. Huang, T.H. Kim, and S.-W. Cheong. *Nature* **418**, 6900, 856 (2002).
- [11] S.T. Bramwell and M.J.P. Gingras. *Science* **294**, 5546, 1495 (2001).
- [12] C. Urano, M. Nohara, S. Kondo, F. Sakai, H. Takagi, T. Shiraki, and T. Okubo. *Phys. Rev. Lett.* **85**, 5, 1052 (2000).
- [13] Y. Horibe, M. Shingu, K. Kurushima, H. Ishibashi, N. Ikeda, K. Kato, Y. Motome, N. Furukawa, S. Mori, and T. Katsufuji. *Phys. Rev. Lett.* **96**, 8, 086406 (2006).
- [14] R.M. Fleming, F.J. DiSalvo, R.J. Cava, and J.V. Waszczak. *Phys. Rev. B* **24**, 5, 2850 (1981).
- [15] F.J. DiSalvo and J.V. Waszczak. *Phys. Rev. B* **26**, 5, 2501 (1982).
- [16] N. Le Nagard, A. Katty, G. Collin, O. Gorochoy, and A. Willig. *J. Solid State Chem.* **27**, 3, 267 (1979).
- [17] T. Sekine, K. Uchinokura, H. Iimura, R. Yoshizaki, and E. Matsuura. *Solid State Commun.* **51**, 4, 187 (1984).
- [18] Si. Ramakrishnan, A. Schönleber, C.B. Hübschle, C. Eisele, A.M. Schaller, T. Rekiş, Nguyen Hai An Bui, F. Feulner, S. van Smaalen, B. Bag, Sr. Ramakrishnan, M. Tolkiehn, and C. Paulmann. *Phys. Rev. B* **99**, 19, 195140 (2019).
- [19] Z.W. Lu, B.M. Klein, E.Z. Kurmaev, V.M. Cherkashenko, V.R. Galakhov, S.N. Shamin, Y.M. Yarmoshenko, V.A. Trofimova, S. Uhlenbrock, M. Neumann, T. Furubayashi, T. Hagino, and S. Nagata. *Phys. Rev. B* **53**, 15, 9626 (1996).
- [20] S. Kawaguchi, Y. Kubota, N. Tsuji, J. Kim, K. Kato, M. Takata, and H. Ishibashi. *J. Phys.: Conf. Ser.* **391**, 1, 2095 (2012).
- [21] S.J. Clark, M.D. Segall, C.J. Pickard, P.J. Hasnip, M.I.J. Probert, K. Refson, and M.C. Payne. *Z. Kristallographie-Crystalline Mater.* **220**, 5–6, 567 (2005).
- [22] Accelrys, Materials Studio CASTEP manual Accelrys (2010).
- [23] P. Hohenberg and W. Kohn. *Phys. Rev.* **136**, 3, B864 (1964).
- [24] J.P. Perdew, A. Ruzsinszky, G.I. Csonka, O.A. Vydrov, G.E. Scuseria, L.A. Constantin, X. Zhou and K. Burke. *Phys. Rev. Lett.* **100**, 13, 136406 (2008).
- [25] D. Vanderbilt. *Phys. Rev. B* **41**, 11, 7892 (1990).
- [26] H.J. Monkhorst and J.D. Pack. *Phys. Rev. B* **13**, 12, 5188 (1976).

- [27] T.H. Fischer and J. Almlof. *J. Phys. Chem.* **96**, 24, 9768 (1992).
- [28] J. Feng, B. Xiao, R. Zhou, W. Pan, and D.R. Clarke. *Acta Materialia* **60**, 8, 3380 (2012).
- [29] Y.D. Zhu, M.F. Yan, Y.X. Zhang, and C.S. Zhang. *Comput. Mater. Sci.* **123**, C, 70 (2016).
- [30] H.M. Tütüncü, E. Karaca, and G.P. Srivastava. *Phil. Mag.* **97**, 29, 2669 (2017).
- [31] M.M. Wu, L. Wen, B.-Y. Tang, L.-M. Peng, and W.-J. Ding. *J. Alloys. Compounds* **506**, 1, 412 (2010).
- [32] J.F. Nye. *Properties Physiques des Materiaux*. Dunod, Paris (1961).
- [33] J. Wang, S. Yip, S.R. Phillpot, and D. Wolf. *Phys. Rev. Lett.* **71**, 25, 4182 (1993).
- [34] M. Born. *Math. Proceed. Cambridge Phil. Soc.* **36**, 2, 160 (1940).
- [35] M.I. Kholil and M.T. Hossen Bhuiyan. *Res. Phys.* **12**, 73 (2019).
- [36] R. Hill. *Proceed. Phys. Soc. A* **65**, 5, 349 (1952).
- [37] Z.-J. Wu, E.-J. Zhao, H.-P. Xiang, X.-F. Hao, X.-J. Liu, and J. Meng. *Phys. Rev. B* **76**, 5, 054115 (2007).
- [38] S. Aydin and M. Simsek. *J. Alloys. Compounds* **509**, 17, 5219 (2011).
- [39] C. Zener. *Elasticity and anelasticity of metals*. University of Chicago Press (1948).
- [40] S.F. Pugh. London, Edinburgh, and Dublin *Phil. Mag. J. Sci.* **45**, 367, 823 (1954).
- [41] J. Haines, J.M. Leger, and G. Bocquillon. *Ann. Rev. Mater. Res.* **31**, 1, 1 (2001).
- [42] T. Ye, Z. Dai, F. Mei, X. Zhang, Y. Zhou, J. Xu, W. Wu, X. Xiao, and C. Jiang. *J. Phys. B* **28**, 43, 434002 (2016).
- [44] H.M. Ledbetter. *J. Phys. Chem. Ref. Data* **6**, 4, 1181 (1977).
- [44] W.-C. Hu, Y. Liu, D.-J. Li, X.-Q. Zeng, and C.-S. Xu. *Comp. Mater. Sci.* **83**, 27 (2014).
- [45] R.S. Mulliken. *J. Chem. Phys.* **23**, 10, 1833 (1955).
- [46] M.D. Segall, R. Shah, C.J. Pickard, and M.C. Payne. *Phys. Rev. B* **54**, 23, 16317 (1996).
- [47] D. Jana, C.-L. Sun, L.-C. Chen, and K.-H. Chen. *Prog. Mater. Sci.* **58**, 5, 565 (2013).
- [48] F. Wooten. *Optical Properties of Solids*. Academic, N.Y. (1972). P. 803–804.
- [49] G. Wang, S. Wu, Z.H. Geng, S.Y. Wang, L.-Y. Chen, and Y. Jia. *Opt. Commun.* **283**, 21, 4307 (2010).
- [50] R. Saniz, L.-H. Ye, T. Shishidou, and A.J. Freeman. *Phys. Rev. B* **74**, 1, 014209 (2006).
- [51] M.L. Ali, M.Z. Rahaman, and M.A. Rahman. *Int. J. Comput. Mater. Sci. Eng.* **5**, 04, 1650024 (2016).
- [52] M. Fox. *Amer. J. Phys.* **70**, 12, 1269 (2002).
- [53] O.L. Anderson. *J. Phys. Chem. Solids* **24**, 7, 909 (1963).
- [54] J.C. Wei, H.C. Chen, W. Huang, and J. Long. *Mater. Sci. Semicond. Proc.* **27**, 883 (2014).
- [55] S. Zhou, J. Long, and W. Huang. *Mater. Sci. Semicond. Proc.* **27**, 605 (2014).
- [56] J. Long, L. Yang, and W. Huang. *Comput. Mater. Sci.* **91**, 315 (2014).
- [57] W. Huang and H. Chen. *Physica B* **449**, 133 (2014).
- [58] M.J. Mehl, B.M. Klein, and D.A. Papaconstantopoulos. *First-principles calculation of elastic properties*. Naval Research Lab, Washington DC (1994).
- [59] D.R. Clarke. *Surface. Coatings Technol.* **163**, 67 (2003).